Shape resonance and non-Franck–Condon effects in (2+1) resonant enhanced multiphoton ionization of O_2 via the $C\,^3\Pi_g$ state

M. Braunstein, J. A. Stephens, and V. McKoy
Arthur Amos Noyes Laboratory of Chemical Physics,[a] *California Institute of Technology, Pasadena, California 91125*

(Received 1 August 1988; accepted 29 September 1988)

We report vibrationally resolved photoelectron angular distributions for photoionization of the $C\,^3\Pi_g$ Rydberg state of O_2. Comparison is made with recent experimental measurements of angular distributions which employ (2 + 1) resonant enhanced multiphoton ionization of the $C\,^3\Pi_g$ state. The present theory treats the process as single-photon ionization from an unaligned Rydberg state, and qualitatively accounts for much of the observed trends. Non-Franck–Condon effects induced by the $k\sigma_u$ shape resonance lead to a substantial dependence of the angular distributions on the vibrational state of the $X\,^2\Pi_g$ ion. Discrepancies between our theoretical results and experiment are qualitatively discussed and tentatively attributed to residual electron correlations.

I. INTRODUCTION

The photoionization dynamics of the $(1\pi_g 3s\sigma_g)$ $^1\Pi_g$ and $^3\Pi_g$ Rydberg states of O_2 have been recently studied using (2 + 1) resonant enhanced multiphoton ionization (REMPI) spectroscopy.[1–3] Analysis of the ion-current and associated photoelectron spectra have yielded the rotational and vibrational constants of these states which are seen to be nearly equivalent to that of the $X\,^2\Pi_g$ ion. In addition they have probed specific electronic interactions with repulsive $(3\sigma_g 1\pi_g^3)$ $^{1,3}\Pi_g$ valence states, which had earlier been investigated by employing electron-impact excitation spectroscopy.[4–7] Most recently, measurements of vibrationally resolved photoelectron spectra of the $v' = 1$–3 levels of the $C\,^3\Pi_g$ state revealed intense, off-diagonal $(\Delta v = v^+ - v' \neq 0)$ peaks for alternative vibrational states of the $^2\Pi_g$ state of the ion.[8,9] This observation was unexpected since for an unperturbed, single-configuration Rydberg state (converging to a specific ion core), the Franck–Condon principle predicts the propensity rule $\Delta v = 0$.[10] The observed non-Franck–Condon behavior was interpreted[8,9] as arising from the formation of a low-energy shape resonance in the σ_u ionization continuum. The dependence of the energy and width of shape resonances on internuclear distance induces strong variations in the electronic transition moment to specific vibrational states of the ion. This mechanism for inducing non-Franck–Condon vibrational distributions was initially investigated in the photoionization dynamics of ground state diatomic molecules.[11–14] The present multiphoton ionization studies of O_2 establish shape-resonant, non-Franck–Condon effects as a prototypical case for study in the context of photoionization of molecular excited states.

In this paper we present studies of photoelectron angular distributions for ionization of the $C\,^3\Pi_g$ Rydberg state of O_2, and also report further details of the *ab initio* calculations published in Ref. 9. Following the measurements[8] and calculations[9] of vibrationally resolved photoelectron spectra, Miller *et al.*[15] have recently measured vibrationally resolved photoelectron angular distributions for photoionization of this same state. Comparison of our calculated angular distributions with the measurements of Miller *et al.* reveal that the σ_u shape resonance, through its angular momentum composition and dependence on nuclear motion, is responsible for much of the observed trends. The present theory treats the process as single-photon ionization from an unaligned Rydberg state, thus neglecting any consideration of alignment arising in the two-photon excitation process. We ascribe the remaining discrepancies between our calculations and experiment to our neglect of alignment of the $C\,^3\Pi_g$ state, and probably more importantly, neglect of electron correlations (beyond the Hartree–Fock level) in the theory. These aspects of the problem are now being investigated, and will be discussed in later publications.

II. THEORY

A. Wave functions and potentials

Within the frozen-core Hartree–Fock approximation, there are four dipole-allowed channels for ionization of the $C\,^3\Pi_g$ state, corresponding to photoionization of the singly occupied $3s\sigma_g$ Rydberg orbital. The electronic continuum wave functions are

$$\Psi(^3\Pi_u) = |[\text{core}]1\pi_g^+ k\sigma_u|\,, \tag{1a}$$

$$\Psi(^3\Sigma_u^+) = \frac{1}{\sqrt{2}}\{|[\text{core}]1\pi_g^+ k\pi_u^-| + |[\text{core}]1\pi_g^- k\pi_u^+|\}\,, \tag{1b}$$

$$\Psi(^3\Sigma_u^-) = \frac{1}{\sqrt{2}}\{|[\text{core}]1\pi_g^+ k\pi_u^-| - |[\text{core}]1\pi_g^- k\pi_u^+|\}\,, \tag{1c}$$

$$\Psi(^3\Delta_u) = |[\text{core}]1\pi_g^+ k\pi_u^+|\,, \tag{1d}$$

where $[\text{core}] = 1\sigma_g^2 1\sigma_u^2 2\sigma_g^2 2\sigma_u^2 3\sigma_g^2 1\pi_u^4$. With these wave functions the static-exchange, one-particle Schrödinger equations for the continuum orbitals can be derived straightforwardly,[16,17] and are of the form

[a] Contribution No. 7822.

 0021-9606/89/020633-08$02.10

$$^3\Pi_u: P\Big[f+\sum_{\text{core}}(2J_i-K_i)+J_{1\pi_g^+}-K_{1\pi_g^+}-\epsilon\Big]P|k\sigma_n\rangle=0 \tag{2a}$$

$$^3\Sigma_u^+: P\Big[f+\sum_{\text{core}}(2J_i-K_i)+J_{1\pi_g^-}-K_{1\pi_g^-}+S''_{1\pi_g}-S'_{1\pi_g}-\epsilon\Big]P|k\pi_u^+\rangle=0\,, \tag{2b}$$

$$^3\Sigma_u^-: P\Big[f+\sum_{\text{core}}(2J_i-K_i)+J_{1\pi_g^-}-K_{1\pi_g^-}-S''_{1\pi_g}+S'_{1\pi_g}-\epsilon\Big]P|k\pi_u^+\rangle=0\,, \tag{2c}$$

$$^3\Delta_u: P\Big[f+\sum_{\text{core}}(2J_i-K_i)+J_{1\pi_g^+}-K_{1\pi_g^+}-\epsilon\Big]P|k\pi_u^+\rangle=0\,. \tag{2d}$$

In these equations J_i and K_i are the Coulomb and exchange operators, and P is a projection operator which enforces orthogonality of the continuum orbital to the occupied orbitals, and ϵ is the photoelectron kinetic energy. The operators S'' and S' are defined by

$$S''_\pi\phi_+(\mathbf{r}_1)=\phi_-(\mathbf{r}_1)\int d^3r_2[\pi_-(\mathbf{r}_2)]^*\frac{1}{r_{12}}\pi_+(\mathbf{r}_2) \tag{3}$$

and

$$S'_\pi\phi_+(\mathbf{r}_1)=\pi_+(\mathbf{r}_1)\int d^3r_2[\pi_-(\mathbf{r}_2)]^*\frac{1}{r_{12}}\phi_-(\mathbf{r}_2)\,, \tag{4}$$

and the one-electron operator in Eq. (2) is

$$f=-\frac{1}{2}\nabla_i^2-\sum_\alpha\frac{Z_\alpha}{r_{i\alpha}}, \tag{5}$$

where Z_α is a nuclear charge.

An iterative procedure for solving the Lippmann–Schwinger equations associated with Eq. (2) has been developed based on the Schwinger variational principle.[16,17] This procedure, discussed in detail elsewhere,[17] begins by solving the Lippmann–Schwinger equations for a separable approximation to the potential U of the form

$$U(\mathbf{r},\mathbf{r}')=\sum_{i,j}\langle\mathbf{r}|\alpha_i\rangle[U^{-1}]_{i,j}\langle\alpha_j|\mathbf{r}'\rangle\,, \tag{6}$$

where the matrix U^{-1} is the inverse of the matrix with elements $U_{ij}=\langle\alpha_i|U|\alpha_j\rangle$ and the α's are discrete basis functions such as Cartesian or spherical Gaussian functions, and U is twice the static-exchange potential in Eq. (2) with the long-range Coulomb potential removed. Solutions obtained with this separable potential can be iteratively improved to yield the converged solutions of the Lippmann–Schwinger equations.[16,17] In this study we used the zero-order solutions, i.e., no iteration, but employed a large basis set $\{\alpha_i\}$ in Eq. (6). Previous studies have shown that such use of a sufficiently large basis ensures convergence of the photoelectron wave function without the need for iterative improvement.

B. Computational details

Determination of the vibrationally resolved cross sections and asymmetry parameters requires the photoionization transition moment, $\langle\Psi_f(\mathbf{r},R)|\mathbf{d}|\Psi_i(\mathbf{r},R)\rangle$, at several values of the internuclear distance R spanning the range of the vibrational motion.[11,18,19] Here $\mathbf{d}$ is the electric dipole operator and $\mathbf{r}$ represents the electronic coordinates. In the adiabatic-nuclei approximation the photoionization cross section for a transition from the v' vibrational level of the $C\,^3\Pi_g$ Rydberg state to the v^+ vibrational level of the $X\,^2\Pi_g$ ion is given by

$$\sigma^{L,V}_{v^+v'}=\frac{4\pi^2}{3c}E\sum_{lm\mu}|\langle\chi(v^+)|I^{L,V}_{lm\mu}|\chi(v')\rangle|^2\,. \tag{7}$$

Here $I^{L,V}_{lm\mu}$ are partial-wave components of the length (L) or velocity (V) incoming-wave normalized transition moment,[18] E is the photon energy, c is the speed of light, and $\chi(v')$ and $\chi(v^+)$ are the vibrational wave functions of the Rydberg state and the ion, respectively. The vibrationally resolved asymmetry parameter $\beta^{L,V}_{v^+v'}$ is defined through the differential photoionization cross section

$$\frac{d\sigma^{L,V}_{v^+v'}}{d\Omega_{\hat{k}}}=\frac{\sigma^{L,V}_{v^+v'}}{4\pi}\left[1+\beta^{L,V}_{v^+v'}P_2(\cos\theta)\right], \tag{8}$$

where θ is the angle between the direction of the light polarization and photoelectron momentum $\mathbf{k}$, and P_2 is a Legendre polynomial of degree two. The transition moments $I^{L,V}_{lm\mu}$ for the $k\sigma_u$ and $k\pi_u$ channels were evaluated at the internuclear distances given in Table I, and interpolated using cubic spline functions. The initial state $C\,^3\Pi_g$ SCF wave functions were calculated using a (9*s*5*p*2*d*/4*s*3*p*2*d*) contracted Gaussian basis set, augmented to include four (with exponents 0.08, 0.02, 0.005, 0.001 25), three (0.05, 0.0125, 0.003 125), and two (0.036 358, 0.010 769) *s*, *p*, and *d*-type diffuse functions, respectively.[4,20–22] The total SCF energy of the $C\,^3\Pi_g$ state at $R=2.282\ a_0$ with this basis is $-149.288\,556$ a.u.

For the final state, we assume the frozen-core Hartree–Fock model, in which the ionic orbitals are constrained to be identical to those of the neutral molecule and the photoelectron orbital is a solution of the one-electron Schrödinger equations given above. For the basis functions α_i in the expansion of Eq. (6) (see Table II) we used Cartesian Gaussian functions centered on each atom and spherical Gaussian functions at the center of mass. All matrix elements in the solution of the Lippmann–Schwinger equations were evaluated using single-center expansions about the center of mass.[17] The partial-wave expansion of the photoelectron or-

TABLE I. Internuclear distances of O_2 where photoionization matrix elements were evaluated.

Photoionization symmetry	Internuclear distance (a.u.)
$3s\sigma_g\rightarrow k\sigma_u$ [a]	1.7,1.894,2.088,2.188,2.238, 2.282 2.311,2.34,2.4,2.588,2.894,3.2
$3s\sigma_g\rightarrow k\pi_u$	1.7,2.088,2.282,2.588,3.2

[a] Shape-resonant channel.

TABLE II. Basis sets used in separable potential, Eq. (6).

Photoionization symmetry	Type of Gaussian function[a]	Exponents
$3s\sigma_g \rightarrow k\sigma_u$	Cartesian s	16.0,8.0,4.0,2.0,1.0,0.5
	z	1.0,0.5
	Spherical $l=1$	4.0,2.0,1.0,0.5,0.25
	$l=3$	4.0,2.0,1.0,0.5,0.25
	$l=5$	1.0,0.5,0.25
$3s\sigma_g \rightarrow k\pi_u$	Cartesian x	16.0,8.0,4.0,2.0,1.0,0.5
	xz	1.0,0.5
	Spherical $l=1$	4.0,2.0,1.0,0.5,0.25
	$l=3$	4.0,2.0,1.0,0.5,0.25
	$l=5$	1.0,0.5,0.25

[a] Cartesian Gaussian basis functions are defined as $\phi^{\alpha,l,m,A}(\mathbf{r}) = N(x-A_x)^l (y-A_y)^m (z-A_z)^n \exp(-\alpha|\mathbf{r}-\mathbf{A}|^2)$ and spherical Gaussian functions are defined as $\phi^{\alpha,l,m,n,A}(\mathbf{r}) = N|\mathbf{r}-\mathbf{A}|^l \exp(-\alpha|\mathbf{r}-\mathbf{A}|^2) Y_{lm}(\Omega_{\mathbf{r}-\mathbf{A}})$. The Cartesian functions are centered on the nuclei and spherical functions are centered on the bond midpoint.

bitals were truncated at $l=7$. The other expansion parameters[16] were chosen as follows:

(i) maximum partial wave in the expansion of the occupied orbitals in the direct potential = 30,

(ii) maximum partial wave in the expansion of the occupied orbitals in the exchange potential = 26 ($1\sigma_g$), 26 ($1\sigma_u$), 14 ($2\sigma_g$), 14 ($2\sigma_u$), 14 ($3\sigma_g$), 14 ($1\pi_u$), 14 ($1\pi_g$),

(iii) maximum partial wave expansion of $1/r_{12}$ in the direct and exchange terms = 60 and 30, respectively,

(iv) maximum partial wave expansion of the nuclear potential = 60,

(v) all other partial wave expansions were truncated at $l=30$.

These parameters provide photoionization cross sections that are within a few percent of the converged values. The associated radial integrals were obtained with a Simpson's rule quadrature. The grid contained 900 points and extended to 96 a.u. with a step size of 0.01 a.u. from the origin to 2.0 a.u. Beyond 2.0 a.u. the largest step size was 0.32 a.u.

For the $C\,^3\Pi_g$ state vibrational wave functions, an RKR potential curve was constructed, and is reported for the first time in Table III, with calculated Franck–Condon factors given in Table IV. The vibrational wave functions for the $X\,^2\Pi_g$ ion were obtained by numerically integrating the RKR potential curve given by Krupenie,[23] in the range of $1.7 \leqslant R \leqslant 3.2$ a.u.

III. DISCUSSION OF RESULTS

A. Fixed-nuclei calculations

In Fig. 1 we show the eigenphase sums for the $3s\sigma_g \rightarrow k\sigma_u$ channel calculated at various internuclear distances. The eigenphase sum δ is given by

$$\delta = \sum_{lm} \arctan(U^\dagger K U)_{lm,lm}\,, \tag{9}$$

where here U is the matrix which diagonalizes the real, symmetric K matrix. A rapid rise of $\sim\pi$ with increasing photoelectron kinetic energy signals the presence of a shape resonance,[14] and examination of the contributions to δ indicates its f-wave ($l=3$) character. The behavior of the eigenphase sum in the $3s\sigma_g \rightarrow k\sigma_u$ channel shows that the resonance is extremely sensitive to changes in R, and in this case extends its spectral variation into the discrete portion of the $k\sigma_u$ channel near the equilibrium bond distance of the ion. Analysis of the fixed-R quantum defects reported by Gerwer *et al.*[24] for $1\pi_g$ photoionization reveals the resonant enhancement of the $n\sigma_u$ Rydberg series which converges to the first ionic threshold. Near-threshold shape resonance behavior was discussed by Raseev *et al.*[25] for the $3\sigma_g$ level of O_2, and by Dittman *et al.*[26] for the $3\sigma_g$ and $1\pi_g$ levels.

The calculated photoionization cross sections for the

TABLE III. Spectroscopic constants and RKR potential energy curve for the $C\,^3\Pi_g$ state of O_2.[a]

$\omega_e = 1951$[b]	$\omega_e x_e = 20.16$[b]	$B_e = 1.68$[c]
$D_e = 4.98\times10^{-6}$[d]	$\alpha_e = 0.0214$[d]	$D_0 = 46264.9$[d]

v'	V	r_{min}	r_{max}
−0.5	0.0	2.1111	
0.0	0.004 423 74	2.031 406 5	2.207 327 2
1.0	0.013 133 18	1.975 560 5	2.280 672 7
2.0	0.021 658 53	1.939 235 4	2.333 778 7
3.0	0.029 999 81	1.911 051 7	2.378 678 5
4.0	0.038 157 02	1.887 658 4	2.418 821 3
5.0	0.046 130 15	1.867 517 0	2.455 777 8
6.0	0.053 919 20	1.849 769 9	2.490 420 8
7.0	0.061 524 18	1.833 881 2	2.523 294 6
8.0	0.068 945 08	1.819 489 4	2.554 766 4

[a] All spectroscopic constants are in cm^{-1}. The potential V, r_{min}, and r_{max} are in a.u.

[b] From Ref. 7.

[c] From Ref. 2.

[d] These constants were obtained from the following relations: $D_e = B_e^3/\omega_e^2$; $\alpha_e = (6\sqrt{\omega_e x_e B_e^3/\omega_e}) - (6B_e^2/\omega_e)$; $D_0 = (\omega_e^2/4\omega_e x_e) - \omega_e/2 - \omega_e x_e/4$.

TABLE IV. Calculated Franck–Condon factors for the transitions O_2 $C\,^3\Pi_g(v') \rightarrow O_2^+$ $X\,^2\Pi_g(v^+)$.[a]

v'	v^+	$\lvert\langle v^+\rvert v'\rangle\rvert^2$
0	0	0.999 845
1	0	$0.416\,395\times10^{-4}$
1	1	0.999 381
1	2	$0.132\,412\times10^{-3}$
2	0	$0.109\,287\times10^{-3}$
2	1	$0.106\,457\times10^{-3}$
2	2	0.995 847
2	3	$0.322\,933\times10^{-2}$
3	0	$0.163\,960\times10^{-5}$
3	1	$0.421\,358\times10^{-3}$
3	2	$0.284\,685\times10^{-2}$
3	3	0.983 515
3	4	$0.123\,974\times10^{-1}$
3	5	$0.699\,919\times10^{-3}$

[a] Franck–Condon factors were obtained with the potential described in Table II for the O_2 $C\,^3\Pi_g$ state, and with the RKR potential of Ref. 23 for the O_2^+ $X\,^2\Pi_g$ state.

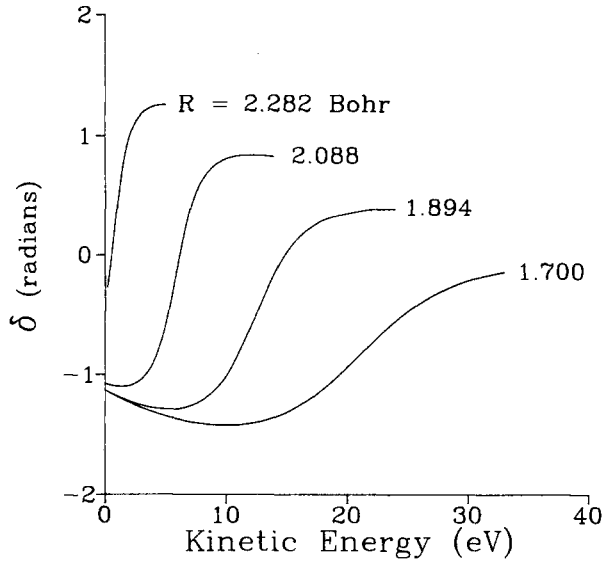

FIG. 1. Calculated eigenphase sums for the σ_u symmetry at various internuclear distances.

$3s\sigma_g \rightarrow k\sigma_u$ channel, shown in Fig. 2, display the corresponding $k\sigma_u$ shape resonance. The R dependence of the transition moment, particularly near the equilibrium bond distance (2.282 a_0) and ~0–2 eV photoelectron kinetic energy, is primarily responsible for the non-Franck–Condon effects observed in the photoelectron angular distributions and branching ratios.

B. Photoelectron angular distributions and branching ratios

In Figs. 3–6 we show our calculated vibrationally resolved photoelectron angular distributions and branching ratios for photoionization of the $v' = 1$–3 levels of the $C\,^3\Pi_g$ Rydberg state. Also plotted are the experimental results of

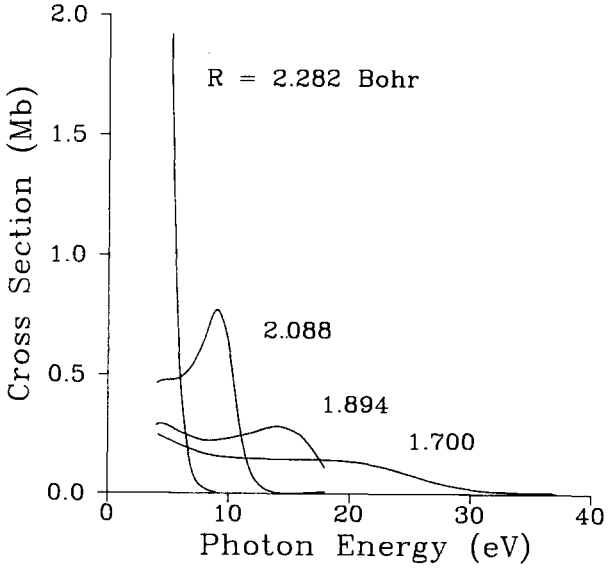

FIG. 2. Calculated (velocity form) photoionization cross sections for the $3s\sigma_g \rightarrow k\sigma_u$ channel at various internuclear distances.

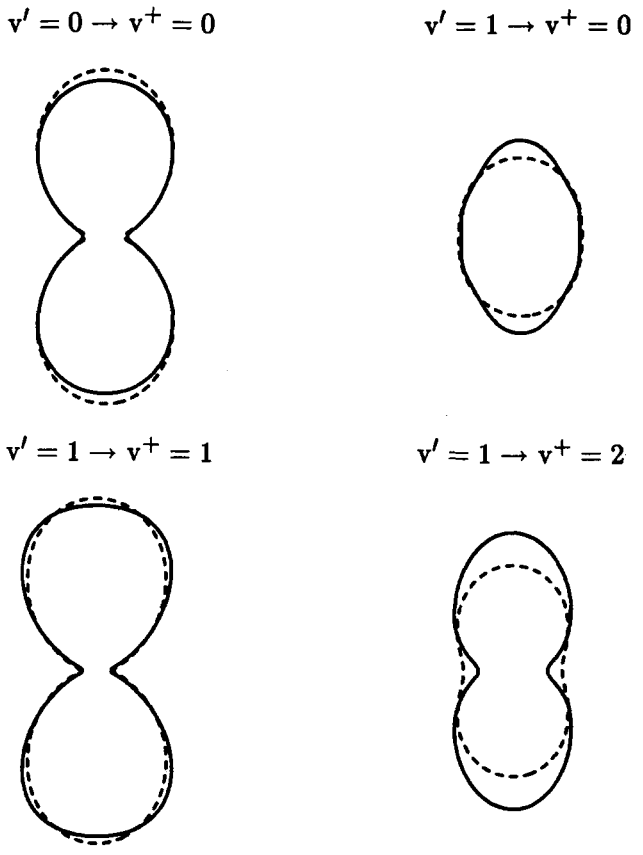

FIG. 3. Calculated (dash curve, velocity form) photoelectron angular distributions for the $v' = 0$ and 1 levels of the $C\,^3\Pi_g$ state, compared with the measurements of Miller *et al.* (Ref. 15, solid curve).

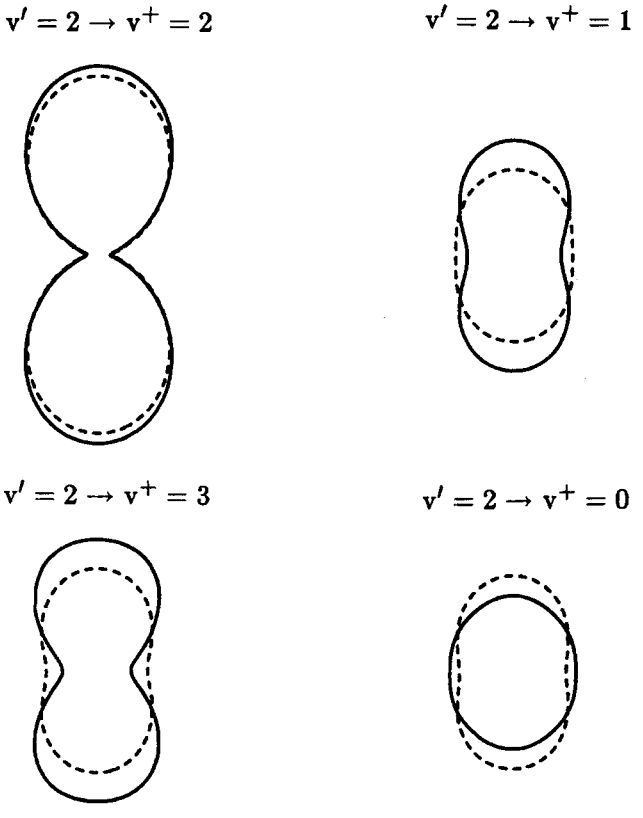

FIG. 4. Calculated (dash curve, velocity form) photoelectron angular distributions for the $v' = 2$ level of the $C\,^3\Pi_g$ state, compared with the measurements of Miller *et al.* (Ref. 15, solid curve).

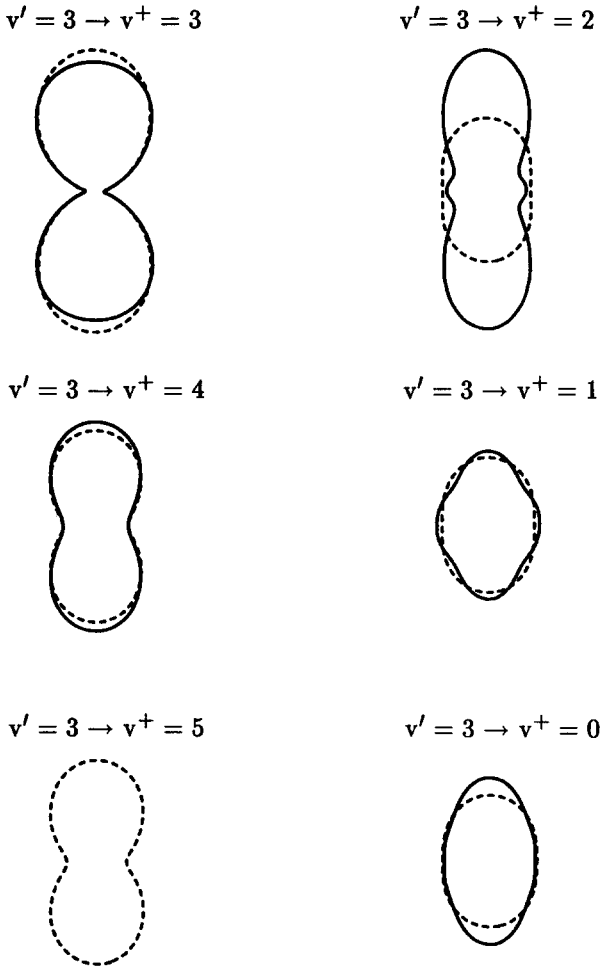

FIG. 5. Calculated (dash curve, velocity form) photoelectron angular distributions for the $v' = 3$ level of the $C\,^3\Pi_g$ state, compared with the measurements of Miller *et al.* (Ref. 15, solid curve).

Miller *et al.*[8,15] Figures 3–5 compare the angular distribution of photoelectron current obtained from theory and the experiment. As shown, each angular distribution is normalized so that in the expansion of the angular distribution, i.e.,

$$\frac{d\sigma}{d\Omega} \propto \sum_{k=0} a_{2k} P_{2k}(\cos\theta) ,$$

the a_0 term equals unity. Note that for an unaligned state only a_0 and a_2 are nonvanishing, and $\beta = a_2/a_0$. The branching ratios have been discussed previously,[8,9] and we include them here (Fig. 6) for completeness, and for comparison with the photoelectron angular distributions. Tables V and VI summarize our calculated results in addition to the measurements.

Referring to Table VI, comparison of our calculated $\beta_{v^+v'}$ asymmetry parameters with experiment shows that results for the diagonal ($\Delta v = 0$) transitions are in near quantitative agreement. Our calculated off-diagonal ($\Delta v \neq 0$) coefficients essentially reproduce the observed trends (smaller a_2 values), however, discrepancies between theory and experiment previously noted[8,9] for the vibrational branching ratios are also apparent here. The most prominent observation in both theoretical and experimental results is the difference in angular distribution between the diagonal and off-diagonal transitions.

The $k\sigma_u$ shape resonance exerts its influence in both diagonal and off-diagonal transitions, and actually constitutes much of the "direct" (i.e., one-electron) transition strength. For example, in the $v' = 1 \rightarrow v^+ = 1$ transition, the $k\sigma_u$ channel accounts for $\sim 53\%$ of the total dipole strength, with the remaining strength partitioned among the $^3\Delta_u$, $^3\Sigma_u^+$, and $^3\Sigma_u^-$ $k\pi_u$ channels. Within the $k\sigma_u$ channel of the $v' = 1 \rightarrow v^+ = 1$ transition, the dipole strength is composed of $\sim 30\%$ f-wave, and $\sim 70\%$ p-wave contributions, the p–f coupling being essential for formation of the shape resonance. Because the $k\pi_u$ channels are nonresonant and hence strongly dominated by the $3s\sigma_g \rightarrow k\pi_u$ ($l = 1$) component at these energies, the angular distributions for the $\Delta v = 0$ transitions display characteristic p-wave-type patterns, as seen in Figs. 3–5 for all diagonal transitions. In contrast, for the *off-diagonal* transitions, the $k\sigma_u$ channel accounts for $\sim 88\%$ of the total ($k\sigma_u + k\pi_u$) dipole strength. The f-wave component of the $k\sigma_u$ resonance causes substantial deviations from "$s \rightarrow p$"-type photoejection (see e.g., the $v' = 1 \rightarrow v^+ = 2$ distribution in Fig. 3). The $3s\sigma_g \rightarrow k\pi_u$ dipole strengths are quite small ($\sim 1\%$–5%) compared to that of the $k\sigma_u$ channel for $\Delta v \neq 0$ transitions, due to the validity of Franck–Condon factorization in these channels. This enormous difference in transition strength for these two continua ($k\sigma_u$ and $k\pi_u$) in $\Delta v \neq 0$ transitions accounts for the calculated and observed differences in the asymmetry parameters.

The a_4 and a_6 coefficients measured by Miller *et al.*[15] become particularly significant for the $v' = 3$ intermediate level, which is also evident by inspection of our Fig. 5. The magnitude of the a_4 and a_6 terms depend on the degree of alignment of the resonant intermediate $C\,^3\Pi_g$ state, as well as the relative phase (and hence interference) between amplitudes for the one-photon ionization step.[27,28] Since the present experiments and theoretical analysis have not attempted to investigate specific rotational excitation branches, it is difficult to rationalize the small magnitudes of a_4 and a_6.

In some cases the magnitude of the discrepancy between the theoretical and measured quantities in Figs. 3–6 appears different whether angular distributions or vibrational branching ratios are compared. For example, the calculated $v' = 3 \rightarrow v^+ = 4$ asymmetry parameter agrees well with the measured value, while the corresponding branching ratio does not. On the other hand, the discrepancies of the calculated $v' = 1 \rightarrow v^+ = 2$ and $v' = 2 \rightarrow v^+ = 3$ asymmetry parameters appear to be consistent with those seen in the branching ratios. Such observations have been documented in single-photon studies,[14] i.e., photoionization dynamics involving shape resonances and electron correlation effects can be mirrored in different ways for the two observables. Since the diagonal transitions are dominated by direct intensity from four continuum channels, electron correlation effects are probably less apparent compared to the off-diagonal transitions, where the single $k\sigma_u$ channel is prevalent. This circumstance permits us to assess the importance of correlation effects in a qualitative, yet preliminary, manner.

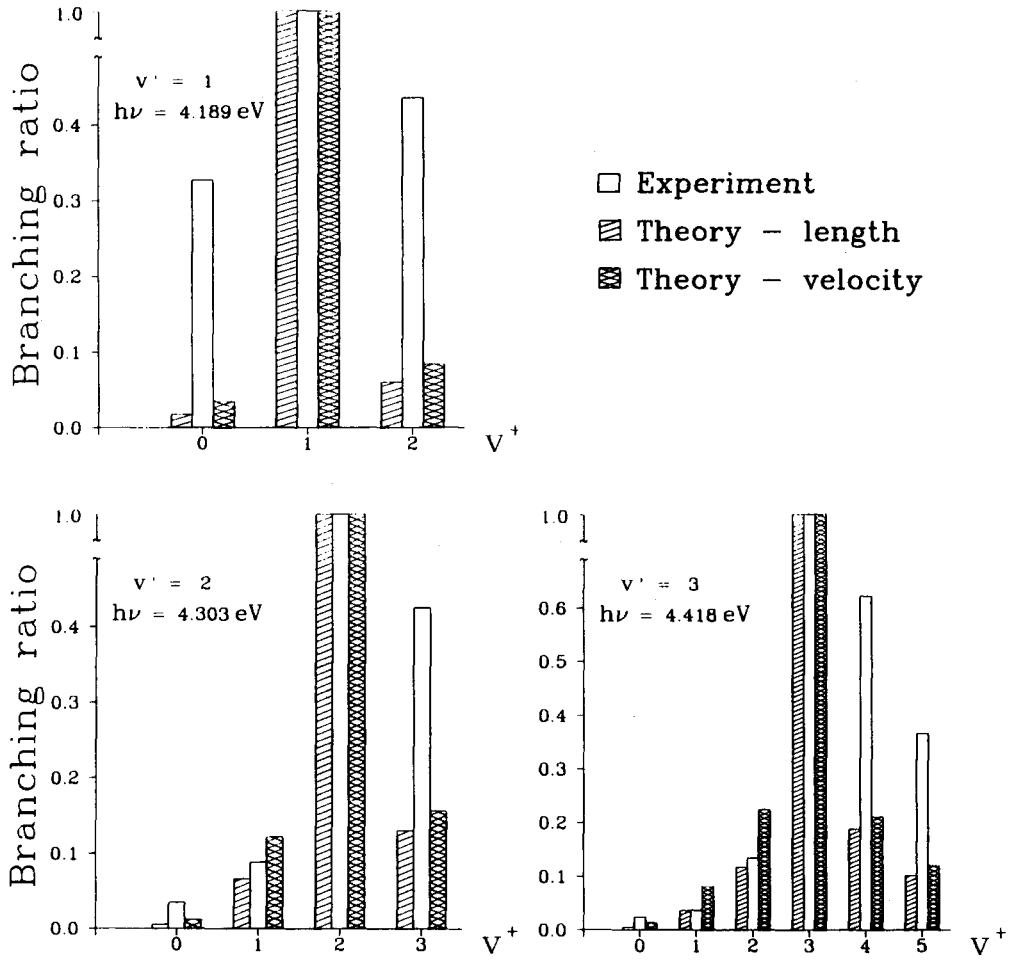

FIG. 6. Calculated vibrational branching ratios for O_2 $C\,^3\Pi_g$ ($v' = 1$–3) photoionization, compared with the measurements of Miller *et al.* (Ref. 8). The theoretical results were normalized to experiment by dividing by the $\Delta v = 0$ peak.

TABLE V. Summary of vibrationally resolved cross sections and branching ratios.

		σ_{v',v^+} (Mb)		$\sigma_{v',v^+}/\sigma(\Delta v=0)$		
v'	v^+	Length velocity (Theory)		Length velocity (Theory)		$\sigma_{v',v^+}/\sigma(\Delta v=0)$ (Experiment[a])
0	0	4.1997	1.3176	1.0000	1.0000	···
1	0	0.0756	0.0495	0.0177	0.0345	0.326
1	1	4.2836	1.4367	1.0000	1.0000	1.000
1	2	0.2580	0.1196	0.0602	0.0833	0.435
2	0	0.0212	0.0158	0.0057	0.0119	0.035
2	1	0.2452	0.1611	0.0660	0.1213	0.088
2	2	3.7172	1.3288	1.0000	1.0000	1.000
2	3	0.4830	0.2068	0.1299	0.1556	0.425
3	0	0.0140	0.0120	0.0052	0.0123	0.024
3	1	0.0964	0.0747	0.0360	0.0808	0.037
3	2	0.3118	0.2068	0.1163	0.2239	0.134
3	3	2.6802	0.9236	1.0000	1.0000	1.000
3	4	0.5027	0.1944	0.1876	0.2104	0.622
3	5	0.2720	0.1101	0.1015	0.1192	0.366

[a] From Ref. 8.

TABLE VI. Summary of vibrationally resolved photoelectron angular distributions.

		β_{v',v^+} (Theory)		
v'	v^+	Length	Velocity	a_2 (Experiment[a])
0	0	1.622	1.456	1.38
1	0	0.128	0.171	0.27
1	1	1.630	1.533	1.66
1	2	0.537	0.551	0.94
2	0	0.394	0.433	0.12
2	1	0.219	0.271	0.67
2	2	1.634	1.629	1.75
2	3	0.618	0.513	1.04
3	0	0.210	0.230	0.36
3	1	0.192	0.264	0.15
3	2	0.197	0.353	0.98
3	3	1.623	1.656	1.64
3	4	0.973	0.794	0.89
3	5	0.877	0.902	···

[a] From Ref. 15. See this reference for a_4 and a_6 coefficients.

C. Electron correlation effects

Several mechanisms which can give rise to anomalous photoelectron spectra of Rydberg states have been pointed out in the literature,[29–34] and recently discussed extensively by Chupka.[10] Such mechanisms may involve one-electron dynamical features (such as the shape resonance in the present study), autoionization of repulsive doubly excited states,[10,29–33] and Rydberg-valence mixing of the resonant intermediate state.[34–37] The latter two mechanisms are many-electron processes requiring theoretical description beyond a Hartree–Fock level for the intermediate bound and continuum final states, respectively. Mechanisms involving many-electron processes have been proposed[8,9] to account for discrepancies between the present calculations and measurements. We discuss them here in more detail to provide a guide for future theoretical effort.

Focusing on the branching ratio results in Fig. 6, there are two (possibly competing) mechanisms which could result in the observed deviations. Earlier experimental evidence suggests[4–6] perturbations of the $v'=1$ level of the $C\,^3\Pi_g$ state, arising from weak configuration interaction with the repulsive $(3\sigma_g 1\pi_g^3)\,^3\Pi_g$ valence state.[22,38] This is corroborated by the MPI spectra of Sur *et al.*,[2] which reveal diffuse (rotationally unresolved) spectra for the low vibrational levels (except for the $v'=2$ band), and is indicative of predissociation. If the ionization step is fast compared to the predissociation induced by the $3\sigma_g 1\pi_g^3$ state, then the relative intensities for the $v'=1$ level should be unaffected. On the other hand, correlation of the repulsive $3\sigma_g 1\pi_g^3$ state with the Rydberg state, viz.

$$\Psi_{\rm Ryd}(R) = C_1(R)\Psi(1\pi_g 3s\sigma_g) + C_2(R)\Psi(3\sigma_g 1\pi_g^3)$$

would introduce an R-dependent coefficient into the effective transition moment,

$$\langle \Psi_k|\mathbf{d}|\Psi_{\rm Ryd}\rangle = C_1(R)\langle k\sigma_u|\mathbf{d}|3s\sigma_g\rangle\,.$$

Buenker and Peyerimhoff[35] have shown that the $C\,^3\Pi_g$ state contains a significant contribution from this repulsive state (near the outer turning point of the $v'=1$ level), in addition to the doubly excited $1\pi_u^2 1\pi_g^3 4\sigma_g$ configuration. Due to the sensitive R dependence already induced in the transition matrix element by the shape resonance, changes in the Rydberg coefficient due to configuration mixing could significantly alter the calculated branching ratios and angular distributions for the $v'=1$ level.

A second mechanism invokes electronic autoionization of dissociative states, which possess many-electron symmetries ($^3\Sigma_u^+$, $^3\Sigma_u^-$, $^3\Delta_u$) associated with the $k\pi_u$ continua accessed from the $C\,^3\Pi_g$ state. (The known states of $^3\Pi_u$ symmetry are inaccessible for autoionization in the present experiments.) The $1\pi_u^3 1\pi_g^3$ electronic configuration gives rise to the $A\,^3\Sigma_u^+$, $B\,^3\Sigma_u^-$, and $C\,^3\Delta_u$ states, which have been studied by accurate *ab initio* calculations,[36–38] particularly in the context of dissociative recombination.[39] Considering these potential curves and the relevant range of internuclear distances (see e.g., Fig. 2 of Ref. 39), the $B\,^3\Sigma_u^-$ state may autoionize leaving O_2^+ in all v^+ levels produced for a given v' excitation. Autoionization of the $A\,^3\Sigma_u^+$ and $C\,^3\Delta_u$ states likely affects only the $v^+=3$–5 levels, produced via the $v'=2,3$ excitations. With the present approximations the $A\,^3\Sigma_u^+$, $B\,^3\Sigma_u^-$, and $C\,^3\Delta_u$ states are not dipole accessible from the $C\,^3\Pi_g$ state (since the configurations differ by two spin orbitals), yet they contribute to autoionization through the dispersion term of the effective transition amplitude or q parameter. Schematically, consider the zero-order states $\psi_E = |1\pi_g k\pi_u|$, $\phi_i = |1\pi_u^3 1\pi_g^3|$, $\Phi_0 = |1\pi_g 3s\sigma_g|$, and the interaction matrix element $V_E = \langle\psi_E|H|\phi_i\rangle$. The resonant continuum wave function Ψ_E is[40,41]

$$\Psi_E = N(E)\{\Phi_i V_E^* + [E - E_i(E)]\psi_E\}\,,$$

where $N(E)$ is a normalization factor (with maximum value at $E=E_i$), and E_i and Φ_i are the *modified* discrete energy and wave function of the autoionizing state ϕ_i. The dipole amplitude between the initial state Φ_0 and the resonant state, and the Fano q parameter are accordingly

$$\langle\Psi_E|\mathbf{d}|\Psi_0\rangle = N(E)V_E^*\Big\{\langle\phi_i|\mathbf{d}|\Phi_0\rangle + P\int_0^\infty dE'\,\frac{V_{E'}^*\langle\psi_{E'}|\mathbf{d}|\Phi_0\rangle}{E-E'} + [E-E_i(E)]\langle\psi_E|\mathbf{d}|\Phi_0\rangle\Big\}\,,$$

$$q = \frac{\langle\phi_i|\mathbf{d}|\Phi_0\rangle}{\pi\langle\psi_E|\mathbf{d}|\Phi_0\rangle V_E^*} + \frac{1}{\pi}P\int_0^\infty dE'\,\frac{1}{E-E'}\,\frac{f(E')}{f(E)}\,,$$

where the function $f(E) = V_E^*\langle\psi_E|\mathbf{d}|\Phi_0\rangle$ and P indicates principal part. For states derived from the $1\pi_u^3 1\pi_g^3$ configuration, the dipole amplitude $\langle\phi_i|\mathbf{d}|\Phi_0\rangle$ vanishes, as noted above. Near the resonance ($E\sim E_i$), contributions to $\langle\Psi_E|\mathbf{d}|\Psi_0\rangle$ are therefore dominated by the dispersion term. This circumstance alone supports the contention of Miller *et al.*[8] that the $B\,^3\Sigma_u^-$ state should appear as a window resonance ($q\sim 0$) in the $k\pi_u$ continuum. On the other hand, contributions to q from the dispersion term actually depend[42] on rapid variations of the *ratio* $f(E')/f(E)$ about the singularity. The resonance profile may change with internuclear distance, depending principally on the R dependence of the matrix element V_E.

IV. SUMMARY AND CONCLUSION

We have presented vibrationally resolved photoelectron angular distributions for photoionization of the $C\,^3\Pi_g$ Rydberg state of O_2. The observed trends in the measured asymmetry parameters are reproduced, in some cases quantitatively, by the theory. The large difference in angular dependence between the diagonal and off-diagonal parameters may be understood by analysis of the contributing degenerate $k\sigma_u$ and $k\pi_u$ ionization channels. Although both $\Delta v=0$ and $\Delta v\neq 0$ transitions are enhanced by the shape resonance, the off-diagonal asymmetry parameters are dominated by contributions from the $k\sigma_u$ channel. Hence the strong f-wave component which is characteristic of the $k\sigma_u$ shape resonance causes substantial deviations from $s\rightarrow p$-type photoejection.

Non-Franck–Condon effects induced by the shape resonance have been identified as an important mechanism which causes striking deviations from the well-known $\Delta v=0$ propensity rule for ionization of molecular Rydberg

states. From the present comparison with measurements, we conclude that specific, multichannel interactions not included in the present theory are also very important. We have tentatively identified these interactions as deriving from configuration mixing of the initial $C\,^3\Pi_g$ state with excited valence states, and autoionization of repulsive valence states derived from the $1\pi_u^3 1\pi_g^3$ electronic configuration. Future theoretical effort should aim at understanding the REMPI dynamics inclusive of these effects.

Finally, due to the ubiquity of shape resonances now documented in single-photon ionization of ground state molecules,[14] we expect them to have important implications for ionization of molecular excited states. Such resonantly induced vibrational distributions strongly influence the preparation of state-selected ions. Indeed, the present studies indicate that vibrational state selection of O_2^+ via the $C\,^3\Pi_g$ state is seriously limited.

ACKNOWLEDGMENTS

The authors acknowledge helpful discussions with Dr. Richard Dubs. This work was supported by grants from the National Science Foundation (CHE-8521391), Air Force Office of Scientific Research (Contract No. 87-0039), and the Office of Health and Environmental Research of the U.S. Department of Energy (DE-FG03-87ER60513). We also acknowledge use of resources of the San Diego SuperComputer Center, which is supported by the National Science Foundation.

[1]A. Sur, C. V. Ramana, and S. D. Colson, J. Chem. Phys. **83**, 904 (1985).
[2]A. Sur, C. V. Ramana, W. A. Chupka, and S. D. Colson, J. Chem. Phys. **84**, 69 (1986).
[3]S. Katsumata, K. Sato, Y. Achiba, and K. Kimura, J. Electron Spectrosc. Relat. Phenom. **41**, 325 (1986).
[4]D. C. Cartwright, W. J. Hunt, W. Williams, S. Trajmar, and W. A. Goddard, Phys. Rev. A **8**, 2436 (1973).
[5]S. Trajmar, D. C. Cartwright, and R. I. Hall, J. Chem. Phys. **65**, 5275 (1976).
[6]R. H. Huebner, R. J. Celotta, S. R. Mielczarek, and C. E. Kuyatt, J. Chem. Phys. **63**, 241 (1975).
[7]T. York and J. Comer, J. Phys. B **16**, 3627 (1983).
[8]P. J. Miller, L. Li, W. A. Chupka, and S. D. Colson, J. Chem. Phys. **89**, 3921 (1988).
[9]J. A. Stephens, M. Braunstein, and V. McKoy, J. Chem. Phys. **89**, 3923 (1988).
[10]W. A. Chupka, J. Chem. Phys. **87**, 1488 (1987).
[11]J. L. Dehmer, D. Dill, and S. Wallace, Phys. Rev. Lett. **43**, 1005 (1979).
[12]R. Stockbauer, B. E. Cole, D. L. Ederer, J. B. West, A. C. Parr, and J. L. Dehmer, Phys. Rev. Lett. **43**, 757 (1979).
[13]J. B. West, A. C. Parr, B. E. Cole, D. L. Ederer, R. Stockbauer, and J. L. Dehmer, J. Phys. B **13**, 1105 (1980).
[14]J. L. Dehmer, A. C. Parr, and S. H. Southworth, in *Handbook on Synchrotron Radiation*, edited by G. V. Marr (North-Holland, Amsterdam, 1986), Vol. II.
[15]P. J. Miller, W. A. Chupka, J. Winniczek, and M. G. White, J. Chem. Phys. **89**, 4058 (1988).
[16]R. R. Lucchese, G. Raseev, and V. McKoy, Phys. Rev. A **25**, 2572 (1982).
[17]R. R. Lucchese, K. Takatsuka, and V. McKoy, Phys. Rep. **131**, 147 (1986), and references quoted therein.
[18]R. R. Lucchese and V. McKoy, J. Phys. B **14**, L629 (1981).
[19]S. N. Dixit, D. L. Lynch, and V. McKoy, Phys. Rev. A **30**, 3332 (1984).
[20]T. H. Dunning, J. Chem. Phys. **53**, 2823 (1971).
[21]J. Andzelm, M. Klobukowski, E. Radzio-Andzelm, Y. Sakai, and H. Tatewaki, in *Gaussian Basis Sets for Molecular Calculations*, edited by S. Huzinaga (Elsevier, Amsterdam, 1984), p. 23.
[22]R. P. Saxon and B. Liu, J. Chem. Phys. **73**, 876 (1980).
[23]P. Krupenie, J. Phys. Chem. Ref. Data **1**, 423 (1972).
[24]A. Gerwer, C. Asaro, B. V. McKoy, and P. W. Langhoff, J. Chem. Phys. **72**, 713 (1980).
[25]G. Raseev, H. Lefebvre-Brion, H. LeRouzo, and A. L. Roche, J. Chem. Phys. **74**, 6686 (1981).
[26]P. M. Dittman, D. Dill, and J. L. Dehmer, J. Chem. Phys. **76**, 5703 (1982).
[27]S. N. Dixit and V. McKoy, J. Chem. Phys. **82**, 3546 (1985).
[28]R. L. Dubs, V. McKoy, and S. N. Dixit, J. Chem. Phys. **88**, 968 (1988).
[29]S. T. Pratt, P. M. Dehmer, and J. L. Dehmer, Chem. Phys. Lett. **105**, 28 (1984).
[30]S. T. Pratt, P. M. Dehmer, and J. L. Dehmer, J. Chem. Phys. **85**, 3379 (1986).
[31]J. C. Miller and R. N. Compton, J. Chem. Phys. **84**, 675 (1986).
[32]A. P. Hickman, Phys. Rev. Lett. **59**, 1553 (1987).
[33]C. Cornaggia, A. Giusti-Suzor, and Ch. Jungen, J. Chem. Phys. **87**, 3934 (1987).
[34]P. J. Miller, L. Li, W. A. Chupka, and S. D. Colson, J. Chem. Phys. **88**, 2972 (1988).
[35]R. J. Buenker and S. D. Peyerimhoff, Chem. Phys. **8**, 324 (1975).
[36]R. J. Buenker and S. D. Peyerimhoff, Chem. Phys. Lett. **34**, 225 (1975); **36**, 415 (1975).
[37]M. Yoshimine, K. Tanaka, H. Tatewaki, S. Obara, F. Sasaki, and K. Ohno, J. Chem. Phys. **64**, 2254 (1976).
[38]R. P. Saxon and B. Liu, J. Chem. Phys. **67**, 5432 (1977).
[39]S. L. Guberman, Int. J. Quantum Chem. Quantum Chem. Symp. **13**, 531 (1979).
[40]U. Fano, Phys. Rev. **124**, 1866 (1961).
[41]A. F. Starace, in *Handbuch der Physik*, edited by M. Mehlhorn (Springer, Berlin, 1982), Vol. 31, pp. 1–121; see especially Sect. III.
[42]U. Fano and J. Cooper, Phys. Rev. **137**, 1364 (1964).